PAPER

Solid-state nanopore based biomimetic voltage gated ion channels

IOP Publishing Bioinspir. Biomim. 12 (2017) 066008 https://doi.org/10.1088/1748-3190/aa811b

Bioinspiration & Biomimetics

PAPER

RECEIVED
9 March 2017

REVISED
17 July 2017

ACCEPTED FOR PUBLICATION
20 July 2017

PUBLISHED
6 November 2017

Solid-state nanopore based biomimetic voltage gated ion channels

Matthew Pevarnik[1,2], Weibin Cui[1], Sukru Yemenicioglu[1], Justin Rofeh[1] and Luke Theogarajan[1]

[1] Department of Electrical and Computer Engineering, University of California, Santa Barbara, Santa Barbara, CA 93106-9560, United States of America

[2] Department of Science and Math, Regent University, Virginia Beach, VA 23464-5037, United States of America

E-mail: ltheogar@ece.ucsb.edu (L Theogarajan)

Keywords: voltage gating, nanopore, biomimetic

Supplementary material for this article is available online

Abstract

Voltage gating is essential to the computational ability of neurons. We show this effect can be mimicked in a solid-state nanopore by functionalizing the pore interior with a redox active molecule. We study the integration of an active biological molecule—a quinone—into a solid state nanopore, and its subsequent induced voltage gating. We show that the voltage gating effect mimics biological gating systems in its classic sigmoidal voltage response, unlike previous synthetic voltage gating systems. Initially, the quinone undergoes a reduction due to radicals in the bulk solution, and is converted to the hydroquinone state. Upon deprontonation the hydroquinone then acts as a charged nanomechanical arm, which opens the channel under the applied potential. We establish that the quinone gains a single net charge when the pH inside of the nanopore reaches its pKa value, and explore factors that influence the net pH in the middle of the pore. Using a combination of theory, experiment and simulation, we conclude that concentration polarization and a shift of the pH inside of the channel is the main cause of this gating effect.

Abbreviations

AQ	Anthraquinone
PNP	Poisson–Nernst Planck
NS	Navier–Stokes
PNP–NS	Poisson–Nernst Planck–Navier–Stokes

1. Introduction

Biological nanopores are sophisticated yet extremely efficient filters, capable of propagating nerve impulses and allowing the passage of specific ions and larger molecules. However, the isolation of biological nanopores can be challenging, and the limitation of experiments performed only under physiological conditions can leave gaps in the depth of study and utilization for emerging technologies. On the other hand, synthetic nanopores are often more robust than their biological counterparts, being able to withstand more extreme conditions (temperature, pH, electrolyte concentration, applied potentials, etc). These devices are then utilized to elucidate the physics of nanoscale transport, as well as serve as a foundation for novel nanoscale devices. Nonetheless, a synthetic channel generally cannot exclude any species, or gain biological functionality outside of steric or electrostatic effects. Thus, a main focus has been in integrating elements of biological pores into synthetic channels, leading to more advanced DNA sequencing, protein sensing, and structure determination, to name a few [1–4]. One particularly interesting area is recreating a voltage-gated channel using synthetic pores. The development of a synthetic voltage gated channel could be particularly useful in regard to controlled drug delivery platforms, nanoscale logic circuits, and more advanced biosensors able to make logical decisions based upon translocating analytes.

Previous attempts to control the flow rate of synthetic pores include attaching a hydrophobic group to the channel interior and entrance, or using a polymer or DNA strand that undergoes a charge transformation at different pH conditions [5–9]. A more immediate and precise method of control than a pH based system is one based upon voltage control. We present a novel system that has a tunable threshold voltage, two distinct conducting states, and mimics properties of certain biological pores like NaChBac, the bacterial sodium channel from *Bacillus halodurans*, and potassium channels in human T-lymphocytes [10–12]. These biological pores show a characteristic sigmoidal voltage gating curve, which was replicated here in a solid state nanopore that was functionalized with 9,10 anthraquinone.

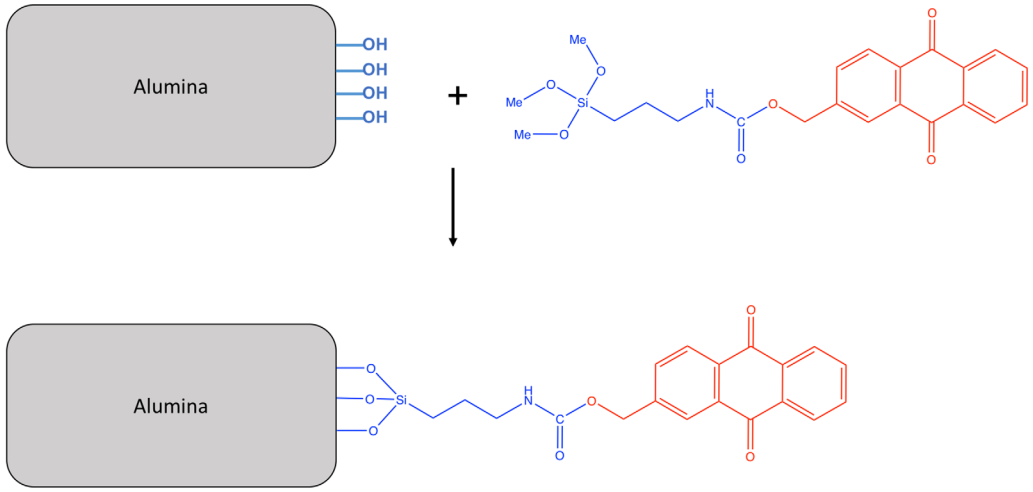

Figure 1. Schematic representation of the functionalized nanopore. Trimethoxysilane terminated anthraquinone, produced by reacting isocyanatopropyltrimethoxysilane and hydroxymethyl anthraquinone, was attached by means of a condensation reaction to the alumina nanopore surface. The anthraquinone moiety is shown in red, and is a common motif found in cancer drugs such as doxorubicin. Linker length was chosen to provide a reasonably flexible linker while ensuring the access to the nanopore interior [18].

Derivatives of quinones appear readily in biologically active molecules, and appear in the electron transport chain as electron acceptors in the processes of photosynthesis and aerobic respiration [13, 14]. Additionally, synthetic quinones appear in anti-tumor or anti-cancer drugs like doxorubicin [15]. These properties make quinone an ideal candidate to study at the single molecule level inside of a nanopore, as well as a strong candidate to add biological-like functionality to otherwise 'normal' synthetic nanopores. Finally, at the nanoscale level it is possible to create drastically different conditions compared to bulk parameters, and thus wildly vary properties like pH and pKa [16], which is explored later in this manuscript.

2. Fabrication

Our fabrication process began with the creation of a 30 nm hole in a commercially available silicon nitride membrane (Norcada Inc.) via a 300 kV TEM. Upon verification of the nanopore creation, the membrane was then subject to a slow-rate, vapor, atomic layer deposition of alumina onto the silicon nitride membrane. The deposition rate was confirmed via TEM to shrink the nanopore inner diameters by 22–26 nm to 4–8 nm (see SI). Further confirmation of the sizing of the nanopores occurred through current–voltage measurements and a fitting of the resistance through equations (2) and (3). Due to silane effectiveness on inorganics being more effective for alumina versus a silicon nitride surface, the silicon nitride surface alone proved less effective. To ensure a clean surface, and assist with nanopore hydration, the entire membrane was immersed in Nano-Strip (KMG Chemicals) for 10 min. The anthraquinone (AQ) was then attached by means of a condensation reaction of siloxane with hydroxy group on membrane surface (figure 1) [17]. Trimethoxysilane terminated anthraquinone was first synthesized by the reaction of hydroxymethyl anthraquinone (Sigma-Aldrich) with isocyanate propyl trimethoxysilane (Gelest, PA). The purified product was dissolved in ethanol at a concentration of about 1 mmol, as stock solvent for the membrane functionalization. The membrane was immersed in the ethanol solution at 60 °C for 1 h. Ethanol was used to assist with nanopore wetting in all pores, especially helping hydrate systems smaller than 5 nm. A schematic of the attachment scheme is shown in figure 1.

2.1. The effect of quinones on nanoscale transport

In addition to the above procedure, separate experiments were performed on the trimethoxysilane group alone. In both cases, the conductance of the nanopore was recorded at 20 kHz (with an Axopatch 200b and HEKA's EPC 10 USB) in response to applied external voltage (ranging from −1000 mV to +1000 mV). While both molecules (the trimethoxysilane group alone and trimethoxysilane terminated AQ) slightly decreased the channel conductance, the trimethoxysilane group alone yielded no additional properties. However, when a sufficiently high stimulus was applied to the trimethoxysilane terminated AQ, the overall ionic current through the nanopore would start to oscillate between a 'closed' and 'open' state. Increasing the applied potential above this threshold would lock the pore in the 'open' state. When the stimulus was taken below the threshold voltage, the gating would reverse and the system would return to its 'closed' state. An ionic current trace of this phenomena at a transition voltage is shown in figure 2. Not shown in figure 2 is the ionic current fluctuating repeatedly between the three states, as this was 2.5 s of a 10.0 s trace. Also seen in figure 2 is a transitionary state in between the 'open' and 'closed' states discussed later in the text.

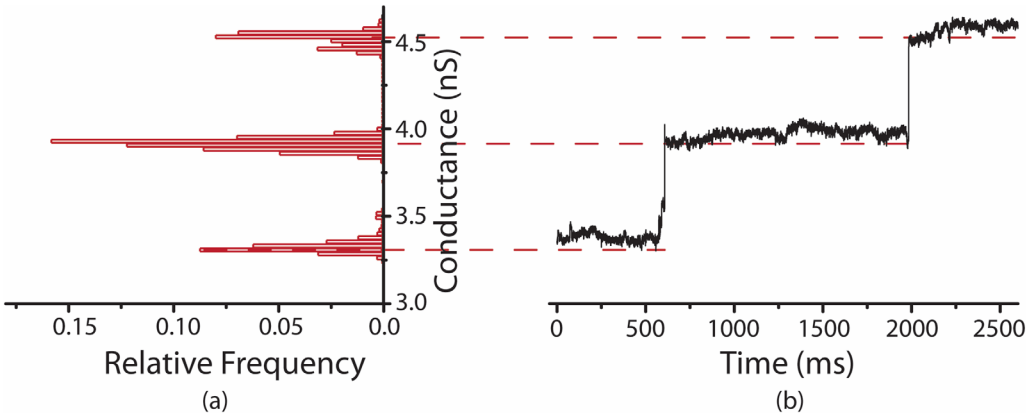

Figure 2. Representative voltage controlled gating behavior in the functionalized solid-state nanopore. The pore diameter was 4.5 nm, and bulk electrolyte was 1 M KCl, 10 mM TRIS buffer, pH 7.4. The successful attachment of the 9,10 anthraquinone resulted in an 'open' and 'closed' conducting state. (a) Histogram of the conductance values obtained at 620 mV applied voltage. Data points were taken by steps of 20 mV from −1000 mV to +1000 mV. The discrete clusters show the quantized nature of the conductance jumps. (b) Current trace versus time at 620 mV applied potential. In this pore, there are distinct intermediate stages between fully open (~4.5 nS) and closed (~2. 6nS) states (see figure 4(b)). Current traces for additional pores can be found in the supporting information (S2) (stacks.iop.org/BB/12/066008/mmedia).

3. Biomimetic voltage gating

Certain types of biological voltage gating are presented on a conductance versus voltage plot, where the conductance of the channel changes between two states [19]. At the threshold voltage, both states are present in equal amounts. Depending on the overall shape of this curve, it is also possible to determine what mechanisms are responsible for biological voltage gating. In equation (1), the energy term is governed by the primary mechanism involved in the gating phenomena. Common gating methods in membrane bound proteins include an intrinsic dipole residue (with $E = \bar{u} \cdot \bar{\varepsilon}$, where $\bar{u}$ is the dipole moment and $\bar{\varepsilon}$ is the electric field) or mobile charges (with $E = qV$, where q is the total mobile charge causing the gating effect, and V is the membrane potential) [20]. A sigmoidal fit can be written as:

$$P_o = \frac{1}{1 + e^{-(E-E_0)/kT}} \quad (1)$$

where P_o is the probability of the channel being open, E_0 is a factor dependent on the threshold voltage, E is the energy of the interaction between the channel and the applied voltage, and kT is the thermal energy of the system. Figure 3 shows a sigmoidal fit to the observed gating, as well as a fit of the energy term to $E = qV$ where q is the elementary charge and $E_0 = qV_T$ with $V_T = 360$ mV. Thus, we established that the AQ gained one elementary charge and changed the overall conductance of the channel, and that the threshold voltage for this nanopore was 360 mV.

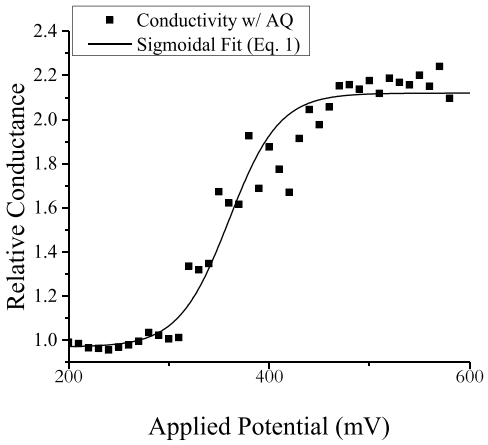

Figure 3. Relative Conductance of AQ modified nanopore. Conductance is scaled to conductance at +200 mV in the 'closed' state (2 nS). For comparison, the open pore conductance prior to functionalization was 6 nS regardless of the applied potential. Sigmoidal fit is using equation (1). Nanopore was 5 nm in diameter with same bulk solution as figure 2.

3.1. Quantized conductivity states

Subsequent experiments revealed either three or four quantized states, though still resulting in sigmoidal voltage gating (see figure 7). There were always at least three states, and at most four states. Two such nanopores, which had inner diameters of 7 nm and 4.5 nm, are shown in figure 4. The 7 nm inner diameter channel had three states, each separated by ~2.0 nS, and the 4.5 inner diameter pore had a total of four states, each separated by ~0.6 nS. Figure 4(a) shows a shift from one low conducting state to three conducting states as the applied potential increased. At this 300 mV threshold, a dwell time analysis reveals no preference between states. Gradually, the lower conducting states disappear, and the nanopore remains in the open state (650 mV). The same can be seen for the 4.5 nm pore (figure 4(b)), except that there are four conducting states. Such specific quantized jumps would not likely occur in a system with a network of quinones (>100 quinones), but would be more likely to occur in the presence of a small number of quinones. It is more

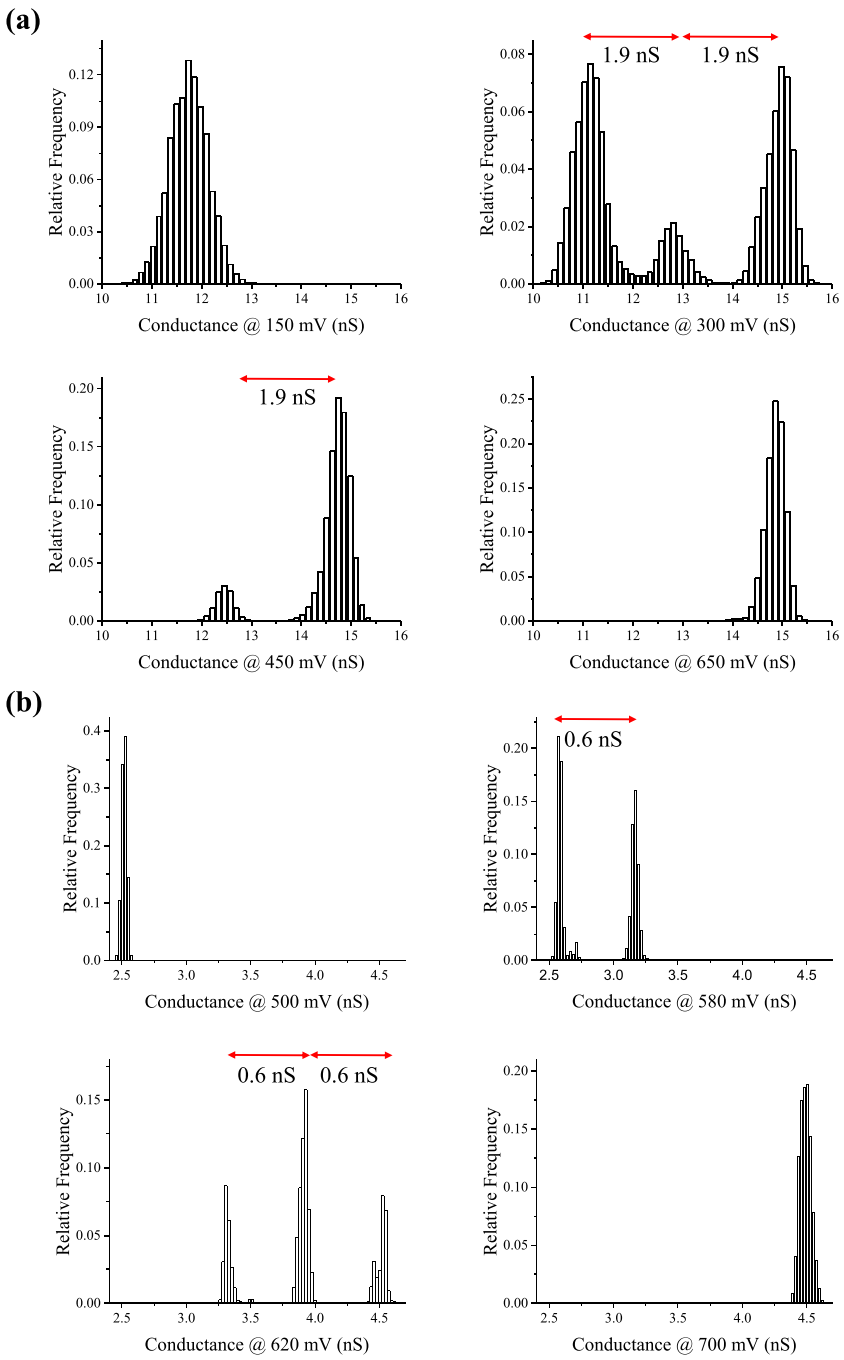

Figure 4. (a) 7 nm pore inner diameter and (b) 4.5 nm pore inner diameter. Data was taken at pH 7.6, 1 M KCl, 10 mM TRIS. Relative count of 1 kHz downsampled signal is plotted versus the conductance of the pore at listed potentials. Quantized conductance jumps are 1.9 ± 0.15 nS for the nanopore in (a) and 0.6 ± 0.02 nS for the nanopore in part (b).

common to attach a small number of target molecules in sub-10 nanometer channels [2], and it is likely one to three quinones are attached to the nanopore interior. If the quinones are attached in different locations inside the nanopore along its vertical axis, and the potential decreases along the nanopore axis, then each quinone will be sitting at a different electric potential. Thus, each quinone does not gain a net charge at the same external potential, and the conductance jumps will be staggered.

3.2. Mechanical opening of channel

In order to explain these quantized jumps and, ultimately, two main conducting states: one of two things is likely occurring. First is a mechanical opening due to a charged quinone anchored to the nanopore interior bending in an electric field (see figure 5). The second is this physical opening plus an increase in conductance due to the increased surface charge density and subsequent electro-osmotic flow. Other gating experiments used a hydrophobic mechanism; however, hydrophobic mechanisms have not shown the ability to produce specific quantized states, and thus the possibility of a hydrophobic mechanism is not explored [5, 6].

A mechanical opening can be explored by considering the resistance of an electrolyte-filled tube of varying cross-section in an insulating membrane:

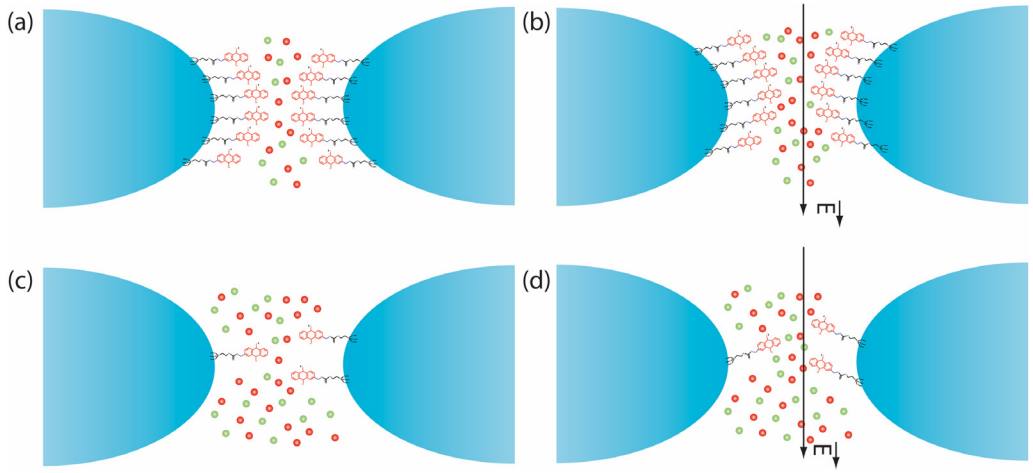

Figure 5. Graphical representation of two schemes proposed in text and plotted in figure 6. Note: these are not perfect representations of the quinone attachments, which would not be as evenly spaced, but rather a visual representation of the schemes proposed in the text. (a) Outlines a network of quinones lining the nanopore interior, (b) opening the channel by 0.3 nm (bending at a 30° angle) when above the opening potential threshold. (c) Three quinones inside of the nanopore opening the channel upon gaining a net charge (d). (c) and (d) Are representative of the neutral molecule below pH 8.9 and the reduced molecule above pH 8.9 respectively, which is described in detail in section 4 of the text.

$$R = 1/\kappa \int \frac{\mathrm{d}z}{\pi r(z)^2} \tag{2}$$

where κ is the electrolyte conductivity and $r(z)$ is the nanopore radius as a function of distance along the nanopore length. Because the nanopores were created via TEM, their overall shape is hyperbolic [21, 22]. The resistance of a hyperbolic nanopore then would be:

$$R_{\mathrm{hyp}} = \frac{2}{\pi\kappa d}\frac{\sin\alpha}{1-\cos\alpha}\tan^{-1}\left(\frac{\sqrt{D^2-d^2}}{d}\right) \tag{3}$$

where d is the diameter of the pore in its narrowest region, D is the diameter of the pore at the mouth opening, α is the asymptotic opening angle of the hyperboloid given by:

$$\sin^2\alpha = \frac{D^2-d^2}{l^2+D^2-d^2} \tag{4}$$

and l is the thickness of the membrane [23]. Comparing the opening ratio to the closed state ratio for several nanopores at pH 7.4 revealed the following. The theoretical fit to the data could be explained by a network of the 1.7 nm long AQ molecule plus linker bending at a 30° angle opening the channel by 0.3 nm more than the closed state (figures 5(a) and (b); figure 6, black). However, as stated above, it is unlikely that a network of AQ molecules is responsible for the effect. Also shown in figures 5(c) and (d) are three quinone molecules extending outwards and bending to a greater degree. There is less agreement with the one–three quinone molecules bending from a purely geometrical standpoint (figure 6, red, blue, green), and a consideration of the effect of electro-osmotic flow is necessary. These results also constrain the limit of our nanopore size, due to declining open to closed state ratios for nanopores larger than 10 nm.

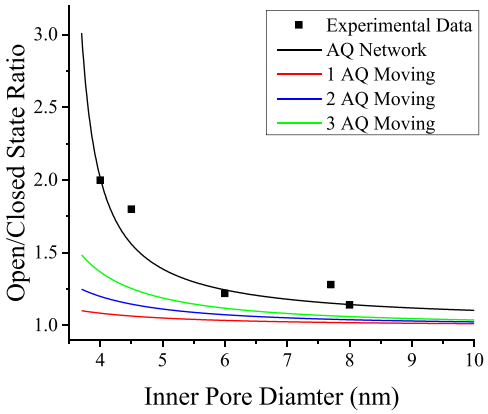

Figure 6. Open to closed state conductance ratio versus inner pore diameter. Five experimental results are all taken at 1 M KCl, 10 mM TRIS, pH 7.4. AQ network plot (black) is derived from equation (3) and is bending at 0.3 nm. One AQ molecule (red), two AQ molecules (blue), and three AQ molecules (green) bending under the electric field is derived from equations (2) and equation (3).

3.3. Effect of electro-osmosis on nanopore current

The effect of electro-osmosis can be determined from the coupled Poisson–Nernst Planck (PNP) and Navier–Stokes (NS) equations. The PNP and NS equations can be written as:

$$\nabla^2\psi = -\frac{\rho}{\epsilon\epsilon_0} \tag{5a}$$

$$J_i = -D_i\left(\nabla C_i + \frac{z_i e C_i}{k_{\mathrm{b}}T}\nabla\psi\right) \tag{5b}$$

$$\nabla\cdot J_i = 0 \tag{5c}$$

$$u\,\nabla u = \frac{1}{\rho}\left[\nu\nabla^2 u - \frac{\rho\nabla\psi}{e}\right] \tag{5d}$$

where:

ψ is the electric potential
ϵ_0 is the permittivity of free space,
ϵ is the relative permittivity of the medium
ρ is the charge density per unit area
J_i is the flux of the ith ion
D_i is the diffusion constant of the ith ion
C_i is the concentration of the ith ion
z_i is the number charge of the ith ion
e is the elementary charge
k_b is the Boltzmann constant
T is the temperature
u is the fluid velocity
ν is the fluid viscosity.

The total current given by a certain density of ions ρ moving at a speed u is given by:

$$i = \int_0^a 2\pi\rho(r)u(r)\mathrm{d}r \tag{6}$$

where a is the inner radius of the nanopore. In the case presented in figure 4, it seems likely that 2(3) quinone molecules were responsible for the 3(4) gating states, and thus $2e(3e)$ of charge would be added the pore. From the NS equation and Poisson equation, we get the velocity of the fluid estimated to be:

$$u(r) = \frac{\epsilon_0\epsilon E_{\text{ext}}}{\nu}(\psi(r) - \zeta_s) \tag{7}$$

where E_{ext} is the external electric field and ζ_s is the zeta potential of the nanopore surface. Rice and Whitehead have solved for the potential in a cylindrical pore [24], which to good approximation can apply when considering only the center of the nanopore. The density of ions is also governed by the Poisson equation such that the nanopore potential and density of ions is:

$$\psi(r) = \zeta_s\frac{I_0(r/\lambda_D)}{I_0(a/\lambda_D)} \tag{8a}$$

$$\rho(r) = -\frac{\epsilon_0\epsilon\zeta_s}{\lambda_D^2}\frac{I_0(r/\lambda_D)}{I_0(a/\lambda_D)} \tag{8b}$$

where λ_D is the Debye length and I_0 is a 0th order modified Bessel function of the first kind. Thus, we can calculate the increase in conductance due to adding one–three electrons' worth of net charge. The result is shown in figure 6, and reveals greater agreement with the experimental data—and makes more physical sense—than a network of quinones moving 0.3 nm. Two of the experimental results fit well to the two-quinone modelu, and three of the experiments fit well to the three-quinone model. This behavior is reflected in histograms of the conductance at different potentials, as illustrated in figure 4. A quantized jump occurs as each quinone gains a net charge, physically bending in addition to increasing the net electro-osmotic current. The maximum conductance occurs once all quinone species are charged, while the minimum conductance occurs when all quinones are in a neutrally charged state.

4. Detecting single molecule reduction/oxidation

The specific mechanism by which each quinone gains a charge is not straightforward. In a traditional cyclic voltammetry experiment, it is simple to explain the addition or removal of net charge from the subject molecule, as it is in direct contact with an electrode that can supply or take away electrons. Anthraquinone has a pKa of ~8.2, and hydroxyanthraquinone has a pKa of ~8.9. However, inside of the nanopore, the anthraquinone has no direct supply of electrons. It is possible that the alumina that is anchoring the quinones is providing an electron, as it has been shown to have redox properties at surfaces—though typically only under extreme temperatures [25, 26]. It is also possible to receive an electron from water if the water can hydrolyze, but that typically occurs at potentials above what our experiment allowed (1400 mV) [27]. Thus, it was greatly puzzling as to how the quinone was gaining a net charge from its neutral state. If the state of the quinone was altered by the presence of radicals in the nanopore solution, then the equilibrium state would be hydroxyanthraquinone (AH). Thus, the following reaction could cause the AH to gain an overall net charge:

$$\mathrm{AH_2} \leftrightarrow \mathrm{AH^-} + \mathrm{H^+}. \tag{9}$$

This reaction would also require there to be a proton acceptor in the solution. In order to test this possibility, a strong radical quencher (ascorbic acid) was added to the *cis* chamber of a gating nanopore. After 30 min the gating began to cease, and the nanopore remained in the 'closed' state. Upon flushing out the channel repeatedly with Millipore water and running the original solution, the gating properties began to return (see SI 3). This is a strong indicator that the quinone is not gaining its charge from the Alumina coating, but rather free radicals in the bulk solution that pass through the channel. The reaction above will proceed once the pH in the quinone region is around 8.9. Shown in figure 7 is gating at different initial bulk pH values. The initiation of this process would therefore not be directly related to the bulk pH of the system (as marked in figure 8), but rather the pH in the nanopore interior, as discussed in the next section of the text.

4.1. Concentration polarization in nanopores

It is possible to have concentration shifts on the nanoscale level, an effect known as concentration polarization [28–30]. In fluidic circuits, while the potential is generated by the external electrodes, the actual potential is set up via the primary charge carriers. Thus, there is a concentration polarization of potassium and chloride that occurs in a region close to the nanopore's opening. Though typically ignored—as protons are rarely a primary charge carrier—there is also a proton gradient across the pore entrance. An example of the proton gradient at 500 mV is shown

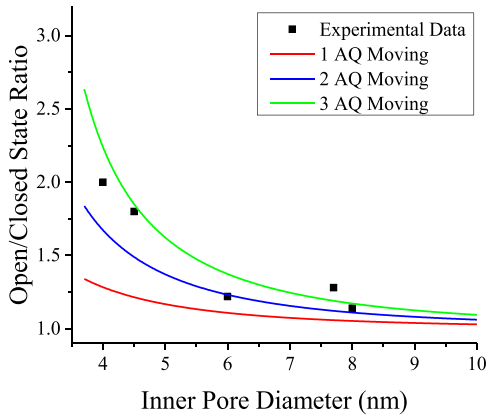

Figure 7. Physical + electro-osmosis model: open/closed state conductance ratio versus inner pore diameter. The updated 'open' state includes the additional electro-osmotic current generated by increase of the net charge inside of the channel by 1–3 elementary charges. Two pores find good agreement with two AQ moving, and three pores find good agreement with three AQ molecules moving. The existence of four and three conducting states respectively for each of these pores provides more validity to the model.

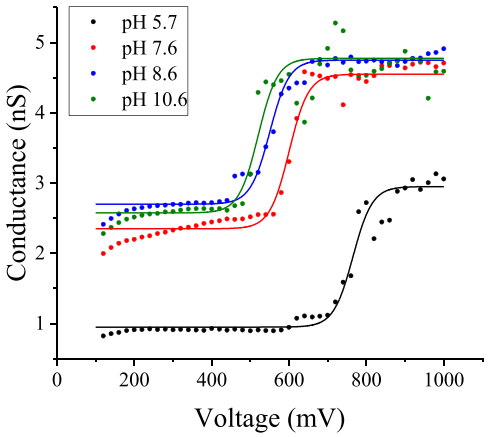

Figure 8. AQ gating at 1 M KCl, pH 5.7, pH 7.6, pH 8.6, and pH 10.6. Sigmoidal fits had opening potential thresholds of 765 mV, 600 mV, 550 mV, and 520 mV respectively. pH 5.7 was unbuffered, and pH 7.6, 8.6, and 10.6 were buffered with 10 mM TRIS and the appropriate amount of 1% NaOH or HCl. The bulk conductivity for each solution was 10.4 mS m^{-1}, 11.4 mS m^{-1}, 11.6 mS m^{-1}, and 11.3 mS m^{-1} respectively, which is not enough to account for the overall lower conductivity at pH 5.7. See supporting information (SI 4) for an explanation of the lower conductivity. Nanopore was 4.5 nm in inner diameter.

using COMSOL in figure 9 whose bulk solution is set to 1 M KCl, pH 7.0. With the bulk conductivity at 1000 mM, the 10 mM TRIS buffer was neglected in COMSOL modeling. In addition to this, the TRIS buffer plays little role in the system other than adding a small amount of overall current and buffering the bulk solution. As seen in figure 9, the pH can shift all the way up to pH 7.7 with the bulk pH fixed at 7.0 based upon the application of the external potential. In order for the quinone to gain a net charge, the pH must be raised up to at least 8.9 for the reaction above to proceed at a favorable rate. However, the potential alone cannot account for shifting the proton concentration inside of the channel for the data presented in figure 8.

Given that the nanopore has between one–three quinones, the majority of the nanopore interior is the Alumina coating, which has a pKa of around 8.9 as well. If the bulk solution is set to pH 7.0, then the Alumina will be positively charged. A positively charged surface would naturally repel excess protons from the nanopore interior, and raise the pH value further, in conjunction with the applied potential. It is possible to calculate the required surface charge density inside of the nanopore using the PNP–NS combined with the applied potential required to recreate the gating phenomena at different pH in figure 8. COMSOL results are shown in figure 10 for the required surface charge density of the Alumina. Also shown in figure 10 is the theoretical surface charge density of the Alumina based upon its pKa values. In order to derive the theoretical surface charge density, we write the set of reactions that occur at the surface of the Alumina:

$$\mathrm{AlOH_2^+} \rightleftharpoons \mathrm{AlOH} + \mathrm{H_s^+} \qquad (10a)$$

$$\mathrm{AlOH} \rightleftharpoons \mathrm{AlO^-} + \mathrm{H_s^+} \qquad (10b)$$

$$\mathrm{AlOH_2^+Cl^-} \rightleftharpoons \mathrm{AlOH} + \mathrm{H_s^+} + \mathrm{Cl_s^-} \qquad (10c)$$

$$\mathrm{AlOH} + \mathrm{K_s^+} \rightleftharpoons \mathrm{AlO^-K^+} + \mathrm{H_s^+} \qquad (10d)$$

where the subscript 's' denotes the surface concentration, which is related to the bulk concentration as:

$$[B_s^{z_i}] = [B_b^{z_i}]\, e^{-\frac{z_i \Psi_0}{kT}} \qquad (11)$$

and B is an arbitrary ion of valence z_i. Reactions of equations (10*a*) and (10*b*) have intrinsic surface ionization constants pK_{a1}^{int} and pK_{a2}^{int} respectively. Reactions of equations (10*c*) and (10*d*) have intrinsic surface complexation constants $*K_{Cl^-}^{int}$ and $*K_{K^+}^{int}$ respectively. Literature values for each are listed in figure 10. From a surface charge standpoint of view, only the concentration of $AlOH_2^+$ and AlO^- on the alumina surface would contribute, with $AlOH_2^+$ being the primary contributor below the point of zero charge (p.z.c.) for alumina (~8.9) and AlO^- dominating when above the p.z.c. If we estimate the surface charge density to be only dependent on $AlOH_2^+$ and AlO^- above and below the p.z.c., respectively, then we can recreate the following alumina surface charge density as shown in figure 10. There is a discontinuity in the graph due to the nature of this estimation breaking down close to the p.z.c., but we see good agreement outside this region.

4.2. Substrate defined voltage tuning

These relations indicate that the alumina (the primary species inside of the nanopore) in combination with the applied potential are responsible for shifting the pH inside of the nanopore to conditions favorable

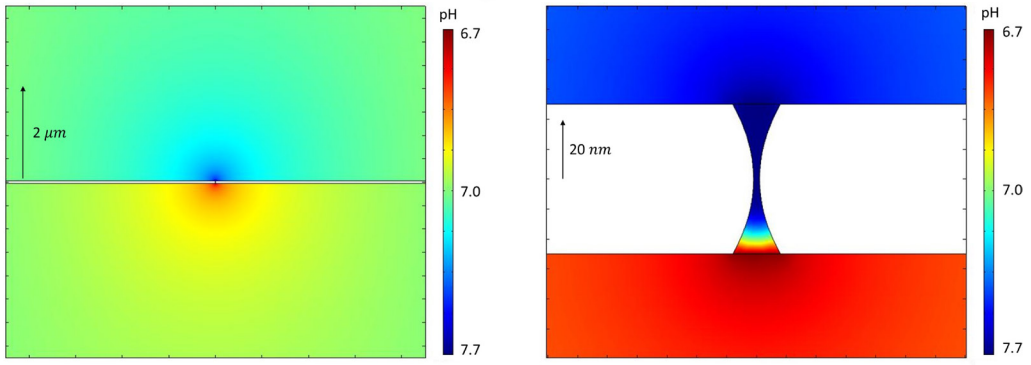

Figure 9. 2D COMSOL modeling of the pH inside of a 4.5 nm inner diameter nanopore. Bulk solution was 1 M KCl, pH 7.0. Applied potential is +500 mV on the upper chamber which results in the pH shifting from 7.0 to 7.7.

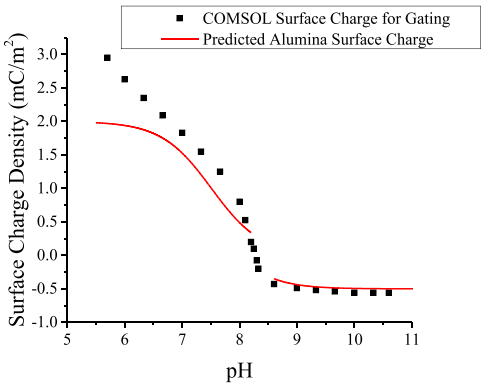

Figure 10. Surface charge density versus pH. The required surface charge density to reproduce the gating shown in figure 7(black) was calculated using the 2D COMSOL geometry from figure 8 and the PNP–NS equations. The theoretical alumina surface charge density was calculated using $pK_{a1}^{int} = *K_{Cl^-}^{int} = 4.4$ and $pK_{a2}^{int} = *K_{K^+}^{int} = 8.9$ (red) [31]. There is a discontinuity due to the estimations being invalid close to the point of zero charge, but we see agreement outside of this region.

for AQH_2 to give up a proton, and become negatively charged. When the bulk pH is above the p.z.c. for alumina (pH ~ 8.3), the surface charge density required to produce the gating does not change much. One way to intuitively understand this phenomenon is to think of alumina acting like a buffer. When the pH of the bulk solution is above the p.z.c., the alumina is almost completely deprotonated—i.e. the equilibrium lies entirely to the right in equation (10*b*)—and contributes protons, thereby restoring to the pH close to the pKa at the interior of the pore. Conversely, when the pH of the bulk is below the p.z.c. the equilibrium lies to the left in equation (10*b*), and the reaction of equation (10*a*) starts being the dominant reaction. As the pH of the bulk falls below the p.z.c. the reaction equilibrium shifts towards the left, removing protons from the solution in the interior of the pore and thereby increasing the pH back towards the p.z.c. Thus, irrespective of the bulk solution pH, the alumina surface buffers the interior of the pore to around 8.2. This large buffering capacity is a direct consequence of the high concentration of alumina within the pore compared to the acid/base concentration. Finally, with the alumina being the primary agent that tunes the pH inside of the nanopore, it is possible to choose a different substrate to line the interior of the pore to tune the opening voltage. If the quinone is switched for another similar molecule with a different pKa, this could also shift the opening potential, and this is a potential avenue of investigation in our lab.

5. Summary

We have shown the ability to create a tunable, classic sigmoidal gating system in an artificial pore, with the ability to control the opening potential. The opening potential can be tuned by the attached molecule, the coating on the inside of the nanopore, or the bulk electrolyte properties. Further investigation remains as to fully explore the effect of other oxides (like a silane coating), the effect of different bulk electrolyte concentrations (which would change the Debye overlap and further effect the pH inside the channel), or another reducible molecule like quinone. This technology can provide a solid foundation for making more advanced synthetic voltage gates—providing great control over the tunability of the gating system, and the ability to precisely control transport rates (in the 'open', 'closed', and intermediate states).

Acknowledgment

This work was supported by the Otis M Williams and Evelyn Freeman Williams Fund at the Santa Barbara Foundation, the NIH Director's New Innovator Award Program (1-DP2-OD007472-01) and the NSF CAREER Award (NSF-CAREER CBET-1056092).

Associated content

Supporting Information includes TEM images of ALD deposition (S1), current traces for other gating nanopores (SI 2), the quenching and restoration with the addition and removal of Ascorbic Acid (SI 3), and

an exploration of the anomalously low current at pH 5.7 from the data presented in figure 7 (SI 4). This material is available free of charge via the Internet.

Author contributions

The manuscript was written with contributions from all the authors. All authors have given approval to the final version of the manuscript.

References

[1] Mohammad M M and Movileanu L 2012 Protein sensing with engineered protein nanopores *Methods Mol. Biol.* **870** 21–37

[2] Wei R, Gatterdam V, Wieneke R, Tampé R and Rant U 2012 Stochastic sensing of proteins with receptor-modified solid-state nanopores *Nat. Nanotechnol.* **7** 257–63

[3] Plesa C, Ruitenberg J W, Witteveen M J and Dekker C 2015 Detection of individual proteins bound along DNA using solid-state nanopores *Nano Lett.* **15** 3153–8

[4] Feng Y, Zhang Y, Ying C, Wang D and Du C 2015 Nanopore-based fourth-generation DNA sequencing technology *Genom. Proteom. Bioinform.* **13** 4–16

[5] Powell M R, Cleary L, Davenport M, Shea K J and Siwy Z S 2011 Electric-field-induced wetting and dewetting in single hydrophobic nanopores *Nat. Nano* **6** 798–802

[6] Pevarnik M, Healy K, Davenport M, Yen J and Siwy Z S 2012 A hydrophobic entrance enhances ion current rectification and induces dewetting in asymmetric nanopores *Analyst* **137** 2944–50

[7] Buchsbaum S F, Nguyen G, Howorka S and Siwy Z S 2014 DNA-modified polymer pores allow pH- and voltage-gated control of channel flux *J. Am. Chem. Soc.* **136** 9902–5

[8] Sachs F and Qin F 1993 Gated, ion-selective channels observed with patch pipettes in the absence of membranes: novel properties of a gigaseal *Biophys. J.* **65** 1101–7

[9] Lev A A, Korchev Y E, Rostovtseva T K, Bashford C L, Edmonds D T and Pasternak C A 1993 Rapid switching of ion current in narrow pores: implications for biological ion channels *Proc. Biol. Sci.* **252** 187–92

[10] DeCoursey T E, Chandy K G, Gupta S and Cahalan M D 1984 Voltage-gated K+ channels in human T lymphocytes: a role in mitogenesis? *Nature* **307** 465–8

[11] Bezanilla F 2000 The voltage sensor in voltage-dependent ion channels *Physiol. Rev.* **80** 555–92

[12] Kuzmenkin A, Bezanilla F and Correa A M 2004 Gating of the bacterial sodium channel, NaChBac *J. Gen. Physiol.* **124** 349–56

[13] Wallace B J and Young I G 1977 Aerobic respiration in mutants of *Escherichia coli* accumulating quinone analogues of ubiquinone *Biochim. Biophys. Acta* **461** 75–83

[14] Allen J P and Williams J C 1998 Photosynthetic reaction centers *FEBS Lett.* **438** 5–9

[15] Cummings J, Willmott N, Hoey B M, Marley E S and Smyth J F 1992 The consequences of doxorubicin quinone reduction *in vivo* in tumour tissue *Biochem. Pharmacol.* **44** 2165–74

[16] Longo G S, Olvera de la Cruz M and Szleifer I 2013 pH-controlled nanoaggregation in amphiphilic polymer co-networks *ACS Nano* **7** 2693–704

[17] Jal P K, Patel S and Mishra B K 2004 Chemical modification of silica surface by immobilization of functional groups for extractive concentration of metal ions *Talanta* **62** 1005–28

[18] Jiang L, Sun Y and Chen X 2012 Chemical reaction on a solid surface with nanoconfined geometry *Small* **8** 333–5

[19] Ehrenstein G and Lecar H 2009 Electrically gated ionic channels in lipid bilayers *Q. Rev. Biophys.* **10** 1

[20] Bezanilla F 2008 How membrane proteins sense voltage *Nat. Rev. Mol. Cell Biol.* **9** 323–32

[21] Kim M J, McNally B, Murata K and Meller A 2007 Characteristics of solid-state nanometre pores fabricated using a transmission electron microscope *Nanotechnology* **18** 205302

[22] Liebes Y, Drozdov M, Avital Y Y, Kauffmann Y, Rapaport H, Kaplan W D and Ashkenasy N 2010 Reconstructing solid state nanopore shape from electrical measurements *Appl. Phys. Lett.* **97** 223105

[23] Kowalczyk S W, Grosberg A Y, Rabin Y and Dekker C 2011 Modeling the conductance and DNA blockade of solid-state nanopores *Nanotechnology* **22** 315101

[24] Rice C L and Whitehead R 1965 Electrokinetic flow in a narrow cylindrical capillary *J. Phys. Chem.* **69** 4017–24

[25] Flockhart B D, Liew K Y and Pink R C 1980 Electron transfer at alumina surfaces. Part 6.—redox properties of fluorided aluminas *J. Chem. Soc. Faraday Trans.* I **76** 2026

[26] Somasundaran P and Li D 2006 *Encyclopedia of Surface and Colloid Science* vol 8, ed P Somasundaran (Boca Raton, FL: CRC Press)

[27] Shen M, Bennett N, Ding Y and Scott K 2011 A concise model for evaluating water electrolysis *Int. J. Hydrog. Energy* **36** 14335–41

[28] Zangle T A, Mani A and Santiago J G 2009 On the propagation of concentration polarization from microchannel-nanochannel interfaces. Part II: numerical and experimental study *Langmuir* **25** 3909–16

[29] Mani A, Zangle T A and Santiago J G 2009 On the propagation of concentration polarization from microchannel − nanochannel interfaces part I: analytical model and characteristic analysis *Langmuir* **25** 3898–908

[30] Yeh H-C, Chang C-C and Yang R-J 2015 Electro-osmotic pumping and ion-concentration polarization based on conical nanopores *Phys. Rev.* E **91** 62302

[31] Todorovic Z and Milonjic S 2004 Determination of intrinsic equilibrium constants at alumina/electrolyte interface *J. Serb. Chem. Soc.* **69** 1063–72